J. Fluid Mech. (1981), *vol.* 108, *pp.* 363–382
Printed in Great Britain

Conditional statistics of Reynolds stress in rough-wall and smooth-wall turbulent boundary layers

By M. R. RAUPACH
Division of Environmental Mechanics, CSIRO, Canberra, Australia

(Received 18 February 1980 and in revised form 13 November 1980)

Quadrant analysis has been used to investigate the events contributing to the Reynolds shear stress in zero-pressure-gradient turbulent boundary layers over regularly arrayed rough surfaces of several different densities, and over a smooth surface. By partitioning the stress into ejections, sweeps, and inward and outward interactions, it is shown that sweeps account for most of the stress close to rough surfaces, and that the relative magnitude of the sweep component increases both with surface roughness and with proximity to the surface. The sweep-dominated region delineates a 'roughness sublayer' with a depth of up to several roughness element heights, in which the turbulence characteristics depend explicitly on the roughness. In the remainder of the inner (or constant-stress) layer, and in the outer layer, the flow obeys familiar similarity laws with respect to surface roughness.

The difference ΔS_0 between the fractional contributions of sweeps and ejections to the stress is shown to be well related everywhere to the third moments of the streamwise and normal velocity fluctuations. Experimental proportionalities are established between the third moments and ΔS_0, and are shown to agree with predictions made from cumulant-discard theory.

The time scale for the passage of large coherent structures past a fixed point, T, is assumed proportional to the mean time between occurrences in a specified quadrant of an instantaneous stress $u'w'$ at least H times the local mean stress $\overline{u'w'}$, where H is a threshold level. For both the ejection and sweep quadrants and for any choice of H, it is found that T scales with the friction velocity u_* and the boundary-layer thickness δ, such that Tu_*/δ is invariant with change of surface roughness.

1. Introduction

The nature of turbulent shear flow close to rough surfaces is of obvious importance in micrometeorology, although its study in an atmospheric context is not as well developed as in engineering applications. Most work on the flow within and just above vegetation canopies, for example, has been based on gradient diffusion models which assume the turbulence to be locally governed. Several atmospheric studies (reviewed by Raupach & Thom 1981) have shown the inadequacy of the approach.

Recent work (Finnigan 1979*a*, *b*) has shown that canopy turbulence is strongly influenced by larger-scale coherent motion in the overlying boundary layer. Such notion has been extensively studied in smooth-wall laboratory boundary layers, most effort being spent on the outer, intermittent region and the wall region (see, for example, recent reviews by Willmarth 1975 and Kovasznay 1977). In the outer layer,

flow visualization (e.g. Falco 1977) and conditional sampling (e.g. Kovasznay, Kibens & Blackwelder 1970), as well as long-established space–time correlation methods, have identified coherent structures associated with the 'bulges' in the turbulent/non-turbulent interface. These structures are quasi-periodic, and occupy the whole boundary-layer depth. They have streamwise and spanwise length scales of the order of 5δ and δ, respectively (δ being the boundary-layer thickness), and live long enough for coherence to be preserved over streamwise distances of 10δ to 20δ. The smooth-wall region, including the viscous sublayer and adjacent buffer layer, has been shown by flow visualization (e.g. Kim, Kline & Reynolds 1971; Nychas, Hershey & Brodkey 1973) to be characterized by a randomly recurring 'burst cycle' in which low-speed fluid near the wall is ejected violently into the overlying flow, immediately followed in time by a downsweep of higher-speed fluid into the region close to the wall. Intense, intermittent Reynolds-stress contributions and turbulence production rates are associated with these 'ejection' and 'sweep' events, as shown with conditional sampling techniques by Wallace, Eckelmann & Brodkey (1972) and Lu & Willmarth (1973). Various authors (e.g. Willmarth & Lu 1974; Kovasznay 1977) speculated that the outer-layer coherent motion is an outgrown manifestation of the bursting process in the wall region, partly on the grounds that the frequencies of both are governed by outer-layer velocity and length scales. More direct evidence for a link between the two comes from the observation of Brown & Thomas (1977) that the mean square fluctuation in wall shear correlates well with low-frequency velocity fluctuation in the outer layer. However, a definite causal sequence has not been established.

There are far fewer studies of boundary-layer turbulence structure over rough surfaces. Grass (1971), using the hydrogen-bubble technique to visualize open-channel turbulent flow over smooth, transitional and rough surfaces, showed that fluid ejections and sweeps both make strong, intermittent contributions to the Reynolds-stress and turbulence production, irrespective of the surface roughness. His observations suggested that the sweep phase is significant only near the wall, whereas the ejection phase is influential through most of the boundary layer. Nakagawa & Nezu (1977) obtained conditional measurements in an open-channel flow which showed that sweeps are more important than ejections in maintaining the Reynolds stress close to rough surfaces.

This paper reports an experimental investigation of the structure of Reynolds stress in wind-tunnel turbulent boundary layers over a smooth surface and several regularly arrayed rough surfaces of different densities. Using an analysis similar to that of Nakagawa & Nezu (1977), it is shown that the relative contributions of ejections and sweeps to the Reynolds stress at a single point are quite well determined by the third moments of the streamwise and normal velocity fluctuations. The sweep-dominated region close to the rough surfaces is clearly identifiable both in the Reynolds-stress conditional statistics and also in the third moments. The paper also discusses the effect of surface roughness on the mean period between occurrences of large contributions to the Reynolds stress by either ejections or sweeps, thereby attempting to infer something of the effect of surface roughness on the large, coherent structures in the overlying boundary layer.

It is convenient at this point to define some terminology. The flow region close to the surface, wherein turbulence statistics depend explicitly on the properties of the roughness, will be called the roughness sublayer. This region forms the wallward part of the inner or surface layer, the remainder of which is the matched layer or 'inertial sublayer'

(Tennekes & Lumley 1972). General statements about the behaviour of turbulence statistics in the roughness sublayer require care, because the mean flow there is three-dimensional for most types of roughness. In principle, a spatial average is required (Raupach & Thom 1981).

We take the co-ordinate axes (x, y, z) to be in the longitudinal, lateral and vertical directions, respectively, with the wall lying in a horizontal plane. The velocity vector is (u, v, w), so that the (negative) Reynolds stress $-\overline{u'w'}$ is the wallward flux density of streamwise momentum. Overbars and primes denote time averages and departures therefrom, respectively.

The wind-tunnel data used here have already been used to investigate the momentum transfer close to rough surfaces from the point of view of flux-gradient relationships (Raupach, Thom & Edwards 1980; hereafter referred to as I). A full account of the experimental details, and an analysis of the simpler mean properties of the flow field, is given there.

2. Theory

To describe the total Reynolds shear stress $\overline{u'w'}$ at a single point as a sum of contributions from different types of events, it is customary to sort instantaneous values of $u'w'$ according to quadrant in the (u', w') plane (e.g. Lu & Willmarth 1973; Wallace *et al.* 1972). We label the events defined by the four quadrants i as outward interactions ($i = 1$; $u' > 0$, $w' > 0$), ejections ($i = 2$; $u' < 0$, $w' > 0$), inward interactions ($i = 3$; $u' < 0$, $w' < 0$) and sweeps ($i = 4$; $u' > 0$, $w' < 0$), respectively. At any point in a stationary flow, the contribution to the total Reynolds stress from quadrant i, excluding a hyperbolic hole region of size H, is

$$\langle u'w' \rangle_{i,H} = \lim_{T \to \infty} \frac{1}{T} \int_0^T u'(t)\, w'(t)\, I_{i,H}[u'(t), w'(t)]\, dt \tag{1}$$

where the angle brackets denote a conditional average, and where the indicator function $I_{i,H}$ obeys

$$I_{i,H}(u', w') = \begin{cases} 1, & \text{if } (u', w') \text{ is in quadrant } i \text{ and if } \quad |u'w'| \geqslant H|\overline{u'w'}|, \\ 0, & \text{otherwise.} \end{cases} \tag{2}$$

The parameter H permits investigation of the contributions to each quadrant of extreme values of $u'w'$. [Note that another definition of H, differing from this one by a factor ρ (the correlation coefficient) is also in common use, e.g. by Lu & Willmarth (1973).] The stress fraction transported by the contribution defined in (1) is

$$S_{i,H} = \langle u'w' \rangle_{i,H} / \overline{u'w'}, \tag{3}$$

and the time fraction during which this contribution is being made is $T_{i,H} = \overline{I_{i,H}(u', w')}$. The definitions imply that $S_{i,H}$ is positive when i is even (sweeps and ejections) and negative when i is odd (the two interaction events). Furthermore,

$$S_{1,0} + S_{2,0} + S_{3,0} + S_{4,0} = 1,$$

since the hole region vanishes when $H = 0$.

The stress fractions $S_{i,H}$ are related to the probability distribution of u' and w', thus: let $p(\hat{u}, \hat{w})$ be the joint probability density function of the rescaled velocity components

$$\hat{u} = u'/\sigma_u, \quad \hat{w} = w'/\sigma_w, \tag{4}$$

where σ denotes a standard deviation, so that $\hat{u}$ and $\hat{w}$ each have unity variance. Then

$$S_{i,H} = \frac{1}{\rho}\int\int_{-\infty}^{\infty} \hat{u}\hat{w}p(\hat{u},\hat{w})I_{i,\rho H}(\hat{u},\hat{w})\,d\hat{u}\,d\hat{w}, \tag{5}$$

where $\rho = \overline{u'w'}/(\sigma_u\sigma_w) = \overline{\hat{u}\hat{w}}$ is the correlation coefficient. Since $p(\hat{u},\hat{w})$ is completely specified by the infinite set of moments

$$M_{jk} = \overline{\hat{u}^j\hat{w}^k} \tag{6}$$

(where j and k are non-negative integers, $j+k$ being the order of the moment M_{jk}), it follows that the moments also determine $S_{i,H}$. In establishing a relationship, it is convenient to consider only the difference

$$\Delta S_H = S_{4,H} - S_{2,H} \tag{7}$$

between stress fractions due to sweeps and ejections, which is a measure of the relative importance of the two types of event.

A specification of ΔS_H in terms of M_{jk} must include moments of at least third order, since a second-order description would make $p(\hat{u},\hat{w})$ Gaussian and hence would give $\Delta S_H = 0$, by symmetry. It will emerge that third-order moments are not only necessary for describing ΔS_H, but also suffice to account for its significant properties. Therefore, we here give a relationship between ΔS_H and the third-order M_{jk} which can be derived by a cumulant-discard method (Antonia & Atkinson 1973; Nakagawa & Nezu 1977). If $p(\hat{u},\hat{w})$ is given by a third-order Gram–Charlier distribution, then

$$\Delta S_H = \frac{1+\rho}{\rho\sqrt{(2\pi)}}\exp\left[-H'(1+\rho)\right]\left[C_1\left(H'^2+\frac{2H'}{1+\rho}+\frac{2}{(1+\rho)^2}\right)+C_2\left(H'+\frac{1}{1+\rho}\right)\right], \tag{8}$$

where $H' = -\rho H/(1-\rho^2)$, and where C_1 and C_2 are two constants constructed from the third-order moments:

$$\left.\begin{aligned} C_1 &= (1+\rho)\,(\tfrac{1}{6}(M_{03}-M_{30})+\tfrac{1}{2}(M_{21}-M_{12})),\\ C_2 &= -(\tfrac{1}{6}(2-\rho)\,(M_{03}-M_{30})+\tfrac{1}{2}(M_{21}-M_{12})).\end{aligned}\right\} \tag{9}$$

An important special case of (8) is

$$\Delta S_0 = \frac{1+\rho}{\rho\sqrt{(2\pi)}}\left[\frac{2C_1}{(1+\rho)^2}+\frac{C_2}{1+\rho}\right], \tag{10}$$

specifying the difference between all stress contributions in the sweep and ejection quadrants, in terms of the third moments. Equations (8) and (10) are obtainable using a variation of the analysis of Nakagawa & Nezu (1977); see, especially, their equations (18)–(29).

3. Experimental details

Full experimental details are given in I, but relevant aspects are summarized here. The data were gathered in a closed-circuit, low (0·1 %) turbulence wind tunnel with a working section 3 m long, 1·33 m wide and 1·22 m high. The experimental boundary layers were formed, with zero pressure gradient, on the upper surface of a splitter plate. Measurements were made over the initial smooth surface and over five rough surfaces sequentially constructed by planting cylindrical roughness elements (of height

Mnemonic	*A*	*B*	*C*	*D*	*E*	*F*
Array type	Smooth	Diamond	Square	Diamond	Square	Diamond
Nearest-neighbour separation D (mm)	—	56·6	40	28·3	20	14·1
Roughness concentration λ (mm)	0	0·011	0·023	0·045	0·090	0·189
Friction velocity u_* (m s^{-1})	0·632	0·843	0·938	1·000	1·025	1·068
Zero-plane displacement d (mm)	0	1	2	3	4	5
Boundary-layer thickness δ (mm)	53	97	120	120	120	126
$\delta_{0\cdot995}$ (mm)	49	90	110	112	112	117
$(h-d)/\delta$	0	0·052	0·033	0·025	0·017	0·008
Reynolds numbers: $(Re_\delta = U_\infty\delta/\nu)$ $\times 10^{-4}$	6·2	11·3	14·0	14·0	14·0	14·7
$R_* = u_* h/\nu$	—	337	375	400	410	427
Total number of runs	8	15	16	16	25	21
Runs used in conditional analysis	Run 10	—	Run 53	—	Run 79	Run 109

TABLE 1. Physical and aerodynamic parameters for the six experimental surfaces, with some details on the data set used here. Quoted values of u_*, d and δ were measured at $x = 2588$ mm, $U_\infty = 17{\cdot}5$ m s^{-1}.

$h = 6$ mm, and diameter 6 mm) in either square or diamond arrays, such that the roughness density was doubled between successive surfaces in the sequence. As in I, the surfaces will be denoted $A, B, \ldots, F$. Table 1 summarizes relevant parameters for each surface. Velocity components were measured with an X-wire anemometer, each signal from which was low-pass filtered at 1·25 kHz and recorded digitally at a scanning rate of 2·5 kHz. A run consisted of readings at 20 positions along a traverse through the boundary layer, 8192 scans being recorded at each position. The results of this paper were all obtained at a free-stream velocity $U_\infty = 17{\cdot}5$ m s^{-1} and at $x = 2588$ mm. (The leading edge of the splitter plate is at $x = 0$, and the plane $z = 0$ is the upper surface of the splitter plate.) For the rough surfaces, all vertical traverses reported here were made at points interstitial to the regular arrays of roughness elements (see I for details).

The normalizing parameters for each surface (the friction velocity u_* and the boundary-layer thickness δ) are given in table 1. Values of u_* were deduced from the Reynolds-stress profiles by assuming that $u_*^2 = -\overline{u'w'}$ in the constant-stress part of each profile; δ was taken as the height at which $\overline{u'w'}$ was 0·5 % of its surface value. For comparison, table 1 also shows values of $\delta_{0\cdot995}$ (based on a velocity defect of 0·5 %). The accuracy of the u_* values is discussed in detail in I.

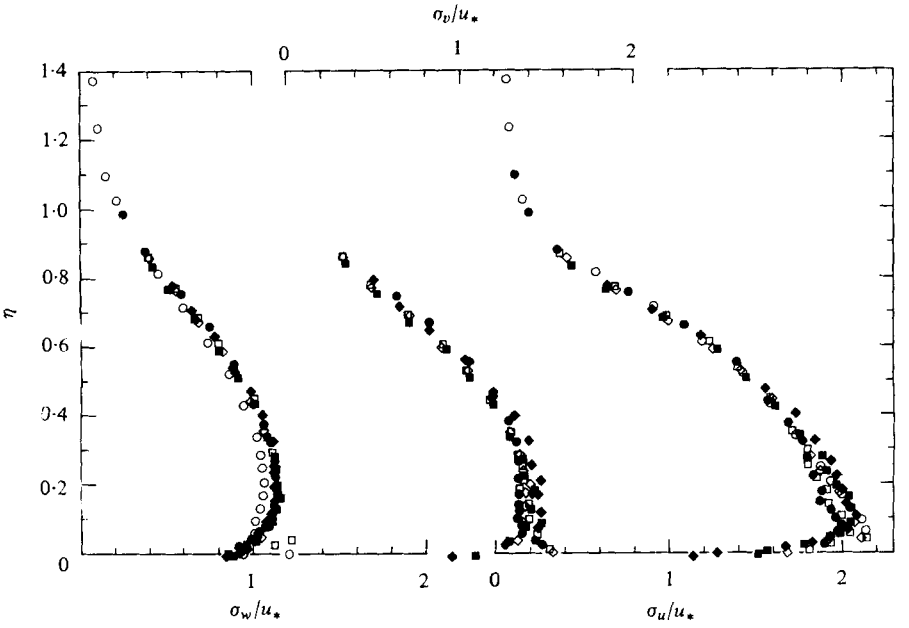

FIGURE 1. Average profiles for each surface of σ_u/u_* (right-hand abscissa), σ_v/u_* (top abscissa) and σ_w/u_* (left-hand abscissa). ○, A; ●, B; □, C; ◇, D; ■, E; ◆, F.

4. Second, third and fourth moments of the velocity fluctuations

Figures 1 and 2 show the average profiles for each surface of the normalized standard deviations of the fluctuating streamwise, lateral and vertical wind components, σ_u/u_*, σ_v/u_* and σ_w/u_*, and of the correlation coefficient $\rho = \overline{u'w'}/(\sigma_u\sigma_w)$. The ordinate is the dimensionless height appropriate to the outer layer, $\eta = (z-d)/\delta$, where d is the zero plane displacement. (The value of η at the top of each roughness canopy is given in table 1; for all surfaces, the roughness occurs below $\eta = 0{\cdot}05$.) The data confirm that, at least for the rough surfaces and outside a region very near the surface (of thickness twice the roughness height at most), normalized second moments of the velocity are universal, roughness-independent functions of η. Data for the smooth surface agree well with these universal curves, except for a tendency in the lower half of the boundary layer for σ_w/u_* to be slightly lower, and hence for ρ to be slightly higher, for smooth than for rough surfaces. These results agree well with data from several other studies (e.g. Antonia & Luxton 1971).

Figure 3 shows average profiles of the third moments of u' and w', presented in the form $M_{jk} = \widehat{u^j}\widehat{w^k} = \overline{u'^j w'^k}/(\sigma_u^j \sigma_w^k)$ where $j+k = 3$, so that M_{30} and M_{03} are the skewnesses of u' and w', respectively. The third moments follow universal curves which are independent of surface roughness, except in a layer close to the surface ($\eta \lesssim 0{\cdot}15$). There, the moments all exhibit roughness dependence such that, at any given height, $|M_{jk}|$ increases with roughness concentration. The near-surface behaviour is made clear in figure 4, in which surface layer data from figure 3 are plotted against height z. (Only four surfaces are represented, for clarity.) Both the extent and the upper height limit of surface influence on M_{jk} appear to depend approximately linearly upon roughness concentration.

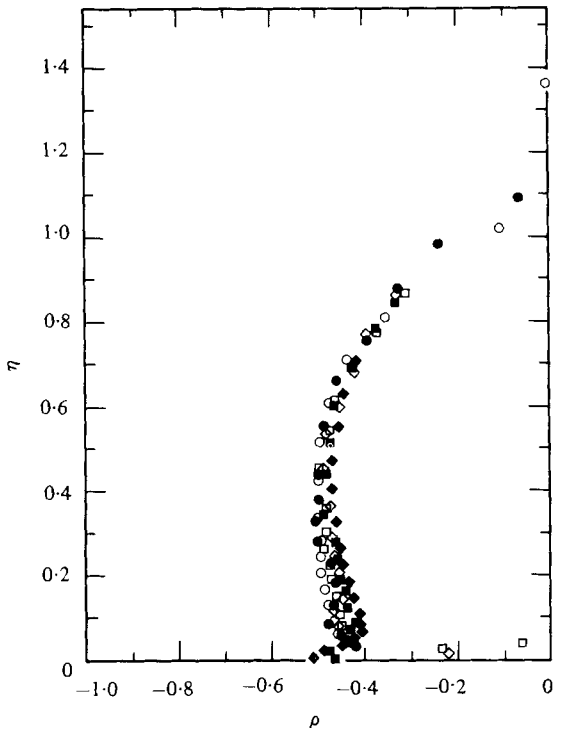

FIGURE 2. Average profile for each surface of the correlation coefficient $\rho = \overline{u'w'}/\sigma_u\sigma_w$. Symbols as in figure 1.

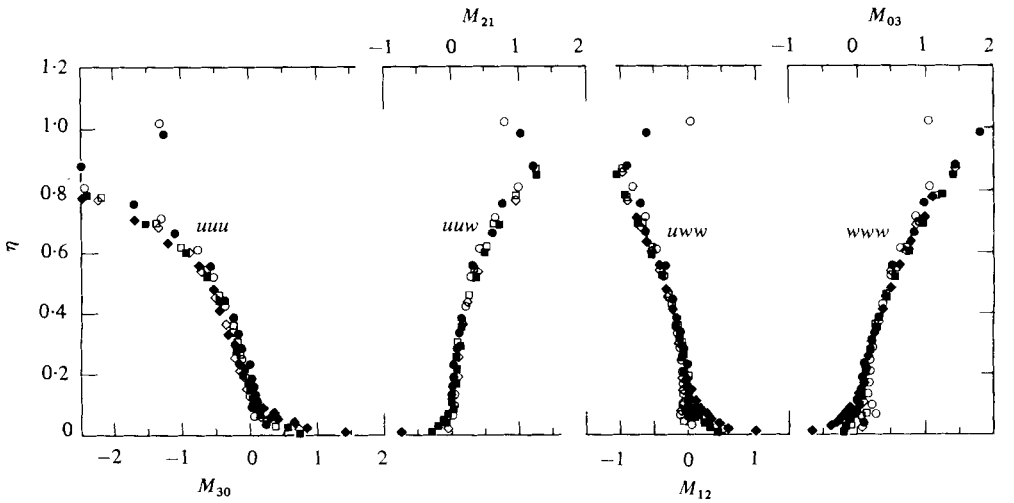

FIGURE 3. Average profiles for each surface of the third moments of u' and w'. Symbols as in figure 1.

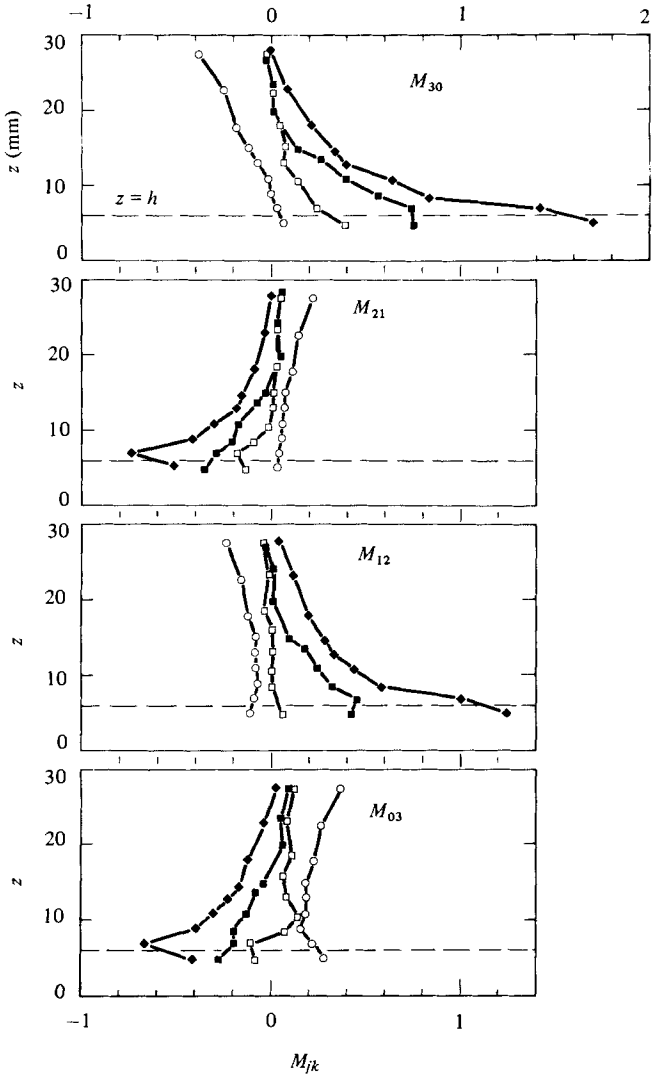

FIGURE 4. Average profiles in the surface layer of the third moments involving u' and w', plotted against height z, for surfaces A, C, E and F. Data replotted from figure 3. ○, A; □, C; ■, E; ◆, F.

Since all the curves in figure 3 have the same shape, a simple proportional relationship applies between the various third moments:

$$M_{30} = -2{\cdot}02M_{21} = 1{\cdot}97M_{12} = -1{\cdot}70M_{03}. \tag{11}$$

The coefficients were deduced by plotting M_{30} against each of M_{21}, M_{12} and M_{03}. They apply to all surfaces, and acceptably describe both the roughness-influenced region and the outer boundary layer. Hence, (11) is generally applicable to the turbulent boundary layers of this experiment.

Figure 5 shows the kurtoses $K_u = \overline{u'^4}/\sigma_u^4$ and $K_w = \overline{w'^4}/\sigma_w^4$ for streamwise and vertical wind fluctuations. Departure from the Gaussian value of 3 is severe only in the outer part of the boundary layer ($\eta \geqslant 0{\cdot}5$).

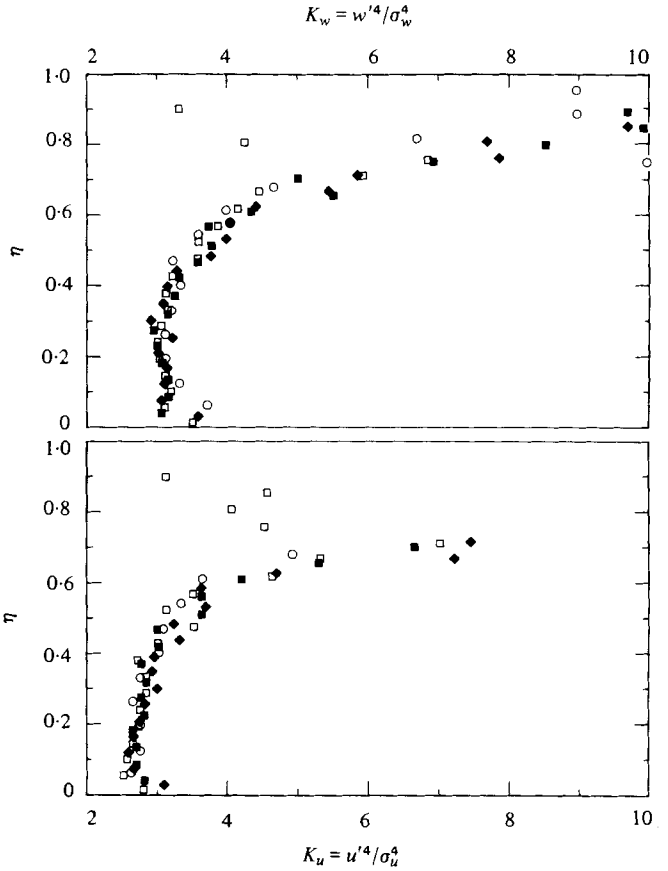

FIGURE 5. Kurtoses K_u (bottom) and K_w (top) for u' and w', for surfaces A, C, E and F. Data from runs 10, 53, 79, 109. Symbols as in figure 4.

5. Conditional statistics of the Reynolds stress

Figures 6 and 7 show stress fractions $S_{i,H}$ plotted against the hole size H for each of the four quadrants in the (u', w') plane. The two figures respectively show results for the smooth surface (A) and the roughest surface (F), at four heights chosen to approximate $\eta = 0{\cdot}05$, $0{\cdot}2$, $0{\cdot}4$ and $0{\cdot}7$; also shown are results for surface F at $z = 3{\cdot}2$ mm, within the roughness canopy. It is evident that, as with the second and third moments of the velocity, the behaviour of $S_{i,H}$ over both surfaces is similar when $\eta \gtrsim 0{\cdot}2$. However, in a region close to the surface, the roughness sublayer, $S_{i,H}$, is strongly dependent on the nature of the surface.

The 'similar' region is discussed first. In its lower part, near $\eta = 0{\cdot}2$, the transport process is relatively symmetric over both surfaces. Ejections and sweeps each contribute about 60 % to the total stress ($S_{2,0} \approx S_{4,0} \approx 0{\cdot}6$) and both remain significant contributors when $H \leqslant 10$. The two interaction quadrants are also symmetric, each contributing about -10 % to the total stress ($S_{1,0} \approx S_{3,0} \approx -0{\cdot}1$), and each ceasing to contribute when $H \geqslant 5$. Comparison with profiles of velocity and Reynolds stress, presented in I, shows that this region of symmetry coincides with the matched layer of 'inertial sublayer', in which the velocity profile is semi-logarithmic and the Reynolds

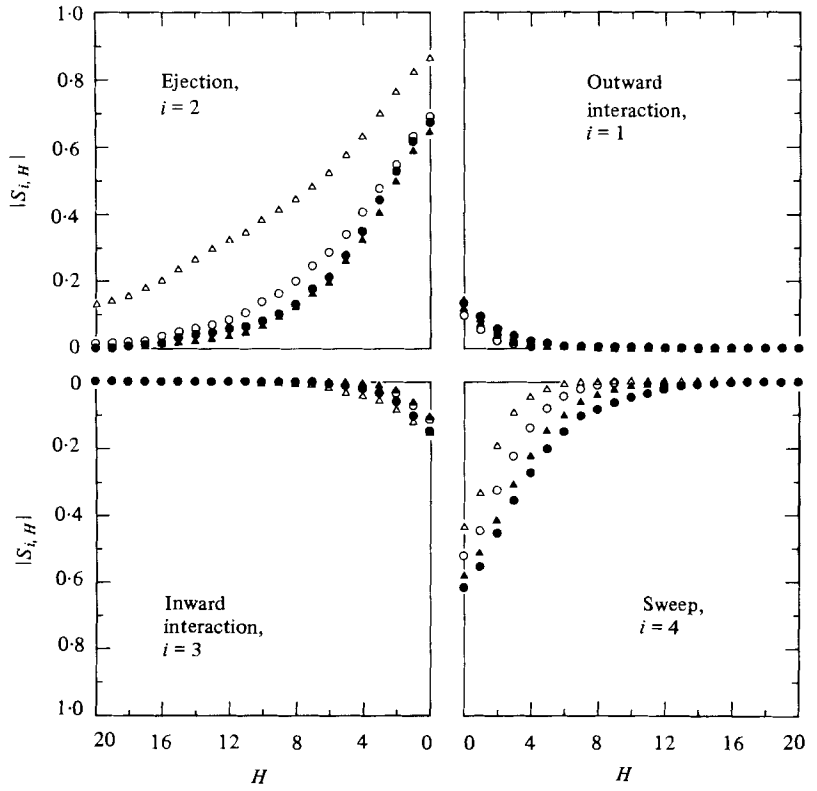

FIGURE 6. Stress fractions $S_{i,H}$ plotted against hole size H, for surface A. ●, η = 0·06; ▲, η = 0·19; ○, η = 0·40; △, η = 0·68. Data from run 10.

stress is approximately constant. On the other hand, the transport process is strongly asymmetric in the outer layer, with ejections becoming progressively more significant as height increases; thus, over both surfaces at $\eta \approx 0{\cdot}7$, ejections account for 90 % of the total stress, and sweeps for 40 %. Also, with increasing η, a progressively increasing stress fraction is contributed at high H values in the ejection quadrant. This general picture is in accord with that established in smooth wall studies (e.g. Lu & Willmarth 1973).

We turn now to the near-surface region. In the case of the smooth surface, the behaviour of $S_{i,H}$ near the surface (at $\eta = 0{\cdot}06$) is similar to that at $\eta \approx 0{\cdot}2$, with ejections and sweeps of comparable importance. Again, this is consistent with earlier observations; Wallace *et al.* (1972) have shown that only in the viscous sublayer ($zu_*/\nu \lesssim 20$, ν being the kinematic viscosity) does the situation change, with sweeps becoming more important than ejections there. Over surface F, however, sweeps are the dominant contributors to the stress both within and above the roughness canopy; when $\eta \leqslant 0{\cdot}03$ or $z \leqslant 9$ mm, sweeps contribute 80 % or more of the total stress. Moreover, sweeps continue to contribute to very large H values ($H \geqslant 20$), whereas ejections entirely cease to contribute when $H \geqslant 3$. This is one of the main distinguishing features of the roughness sublayer; later, it will be shown to occur also over other types of rough surface.

Because significant fractions of stress are transported at high values of H, especially

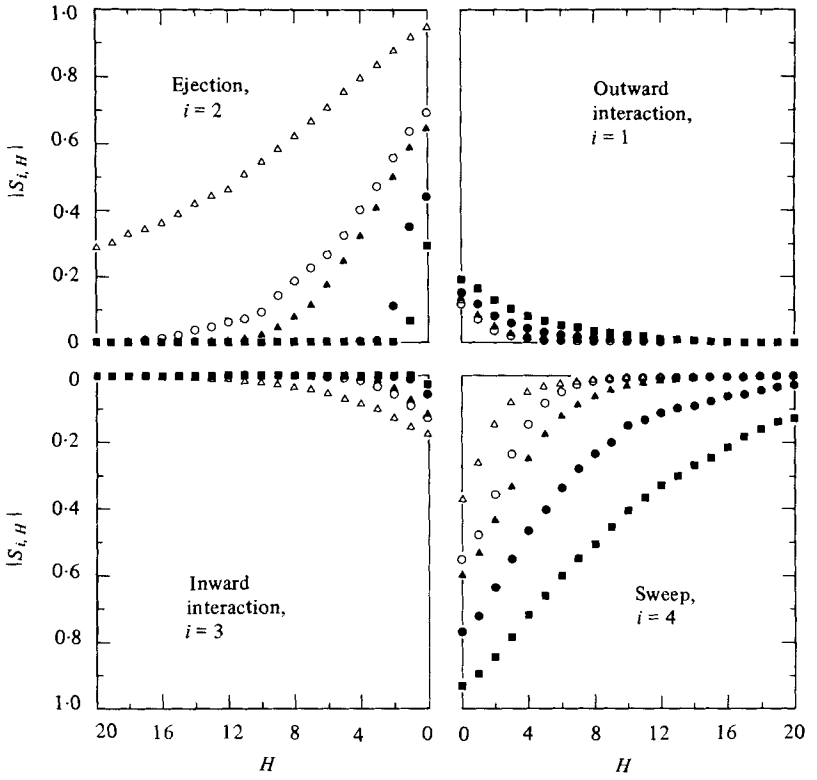

FIGURE 7. Stress fractions $S_{i,H}$ plotted against hole size H, for surface F. ■, within roughness canopy (z = 3·2 mm); ●, η = 0·03; ▲, η = 0·21; ○, η = 0·39; △, η = 0·71. Data from run 109.

	Ejection (i = 2)		Sweep (i = 4)	
H	$S_{i,H}$	$T_{i,H}$	$S_{i,H}$	$T_{i,H}$
0	0·287	0·480	0·930	0·247
5	0	0	0·660	0·061
10	0	0	0·404	0·025
20	0	0	0·128	0·005
30	0	0	0·051	0·001

TABLE 2. Stress fractions $S_{i,H}$ and time fractions $T_{i,H}$ for surface F, z = 3·2 mm (within the roughness canopy).

in the roughness sublayer and the outer layer, the transport process is highly intermittent, in the sense that much of the stress is transported during periods of strong turbulence activity which occupy a small fraction of the time. Table 2 shows the time fractions taken by sweep and ejection events at various hole sizes, using the flow over surface F at z = 3·2 mm (within the canopy) as an example. Sweeps with $H \geqslant 10$ account for 40 % of the stress in 2·5 % of the time; at $H \geqslant 20$, sweeps account for 13 % of the stress in 0·5 % of the time. In the outer layer, the ejection quadrant displays a similar behaviour.

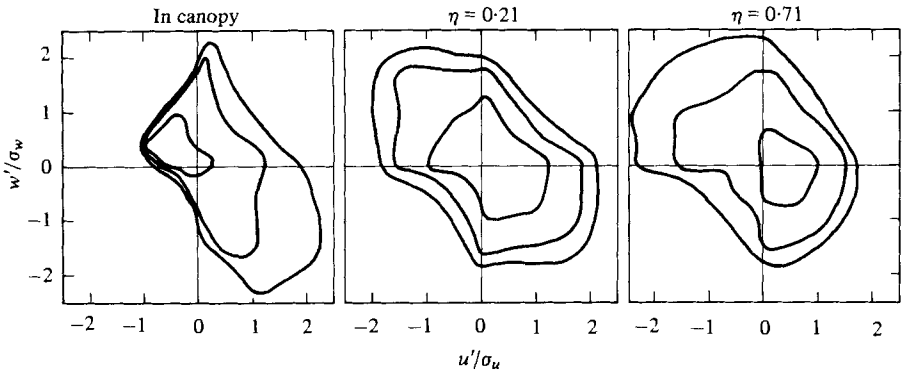

FIGURE 8. Joint probability density function $p(\hat{u},\hat{w})$ at three different heights over surface F. Contours denote probabilities of 50%, 20% and 10%. Data from run 109.

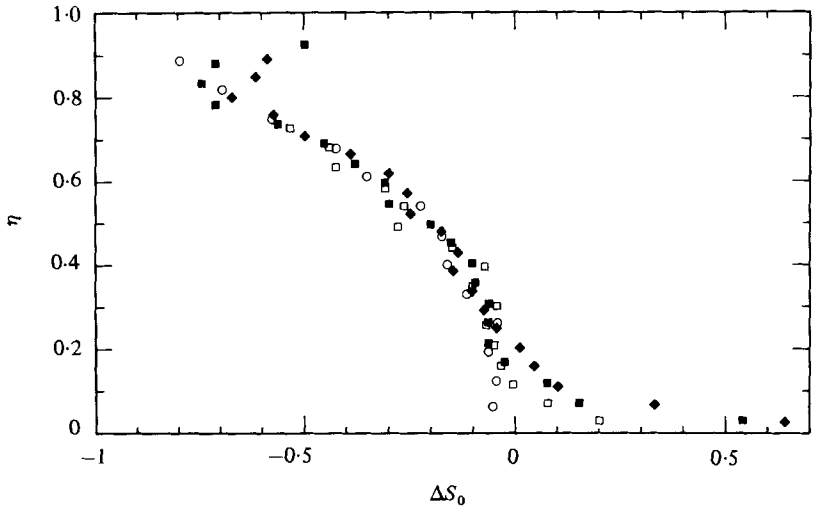

FIGURE 9. The difference ΔS_0 between sweep and ejection stress contributions, for surfaces A, C, E and F. Data from runs 10, 53, 79, 109. Symbols as in figure 4.

Since the behaviour of $S_{i,H}$ is determined entirely by the joint probability density function $p(\hat{u}, \hat{w})$, through (5), it is helpful to examine $p(\hat{u}, \hat{w})$ itself. Figure 8 shows contours of $p(\hat{u}, \hat{w})$ at three different heights over surface F. As height increases from the canopy region to the outer layer, there is a clear shift in the most favoured location for large values of $-\hat{u}\hat{w}$ from the sweep quadrant to the ejection quadrant. In the matched layer ($\eta \approx 0{\cdot}2$), contours of $p(\hat{u}, \hat{w})$ resemble the concentric ellipses of the joint Gaussian distribution, except for a tendency for $\hat{u}$ and $\hat{w}$ to inhibit each other in the inward and outward interaction quadrants. This effect was consistently observed in the present data set over all surfaces including the smooth surface, A; its statistical significance is beyond doubt but the cause remains unknown.

The most important features of the above results for $S_{i,H}$ can be described succinctly by the single parameter $\Delta S_0 = S_{4,0} - S_{2,0}$, the fractional difference between stress contributions by sweeps and ejections. Figure 9 shows the variation of ΔS_0 with η for surfaces A, C, E and F. It is immediately clear that, outside the roughness sublayer,

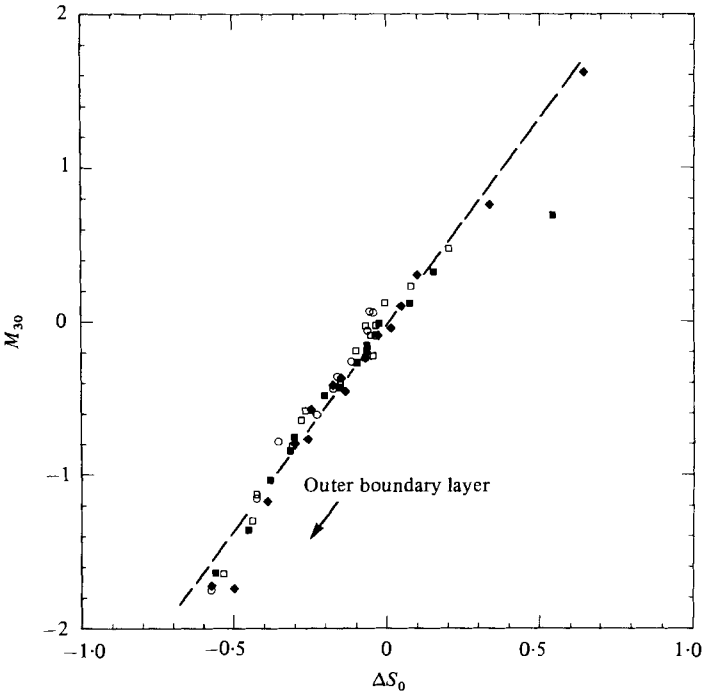

FIGURE 10. M_{30} plotted against ΔS_0. Data from runs 10, 53, 79, 109. The dashed line is the proportionality $\Delta S_0 = 0{\cdot}37 M_{30}$. Symbols as in figure 4.

ΔS_0 is independent of surface roughness; this conclusion has been anticipated above. On the other hand, within the roughness sublayer, ΔS_0 increases with roughness concentration from near zero for surface A to more than 0·5 close to surfaces E and F. The tendency for sweeps to dominate momentum transfer over a rough surface is therefore strongly dependent upon the roughness concentration, being greatest when the roughness concentration is highest.

Figure 9 also demonstrates the strong resemblance between the height dependence of ΔS_0 and that of the third moments M_{jk} (shown in figure 3). This is a consequence of the relationships (8) and (10) between ΔS_H (or ΔS_0) and the third moments, which may be tested quantitatively as follows.

In figure 10, M_{30} (the skewness of u) has been plotted against ΔS_0, for runs A, C, E and F. To a good approximation, a single proportionality relates the two quantities everywhere in the boundary layer, and for all surface types. The other third-order moments, when plotted against ΔS_0, demonstrate similar linear relationships. The dashed line in figure 10 represents the proportionality

$$\Delta S_0 = 0{\cdot}37 M_{30}. \tag{12}$$

A prediction of the slope of this line can be made from (10), together with the observed relationships (11) among the third-order M_{jk} and an approximate correlation coefficient $\rho = -0{\cdot}45$, assumed to apply at all heights and roughnesses (cf. figure 2). The result is $\Delta S_0 = 0{\cdot}34 M_{30}$, which is in acceptable agreement with (12). Hence, quite a good description of the ejection–sweep character of boundary-layer turbulence (parametrized by ΔS_0) can be obtained by considering moments of u' or w' up to third order only.

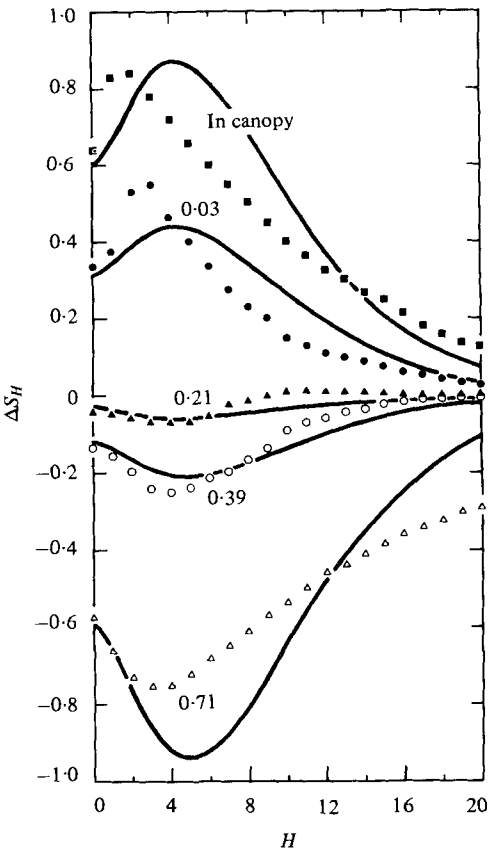

FIGURE 11. Calculated and observed values of ΔS_H, at the same five heights over surface F as represented in figure 7. Data from run 109; symbols as in figure 7.

A more stringent test of the third-order theory is shown in figure 11. For five heights over surface F, identical with the heights represented in figure 7, observed values of ΔS_H are plotted against H. Also plotted are the predictions from (8), obtained using the measured correlation coefficient and third moments for each level. The agreement at $H = 0$ is good for all levels, but systematic discrepancies appear between theory and observation at higher values of H. This is not surprising, as progressively higher moments are needed to specify the distribution – and hence $S_{i,H}$ and ΔS_H – as values of H become larger. It is, of course, possible to extend equation (8) to include higher-order moments, hence improving the fit in figure 10; Antonia & Atkinson (1973) have thoroughly investigated this as a method for specifying the Reynolds stress distribution in terms of its own skewness and kurtosis. However, a specification of ΔS_H – and, particularly, of ΔS_0 – at third order is practically useful, for at least two reasons. First, the turbulent energy flux is thereby related to the local ejection or sweep character of the stress (see later). Second, a third-order relationship is usually all that can be applied in the atmosphere, where problems of non-stationarity make fourth- and higher-order moments very difficult to measure reliably. Later, we give a brief comparison of the present third-order results with data from roughness sublayer flows in the atmosphere.

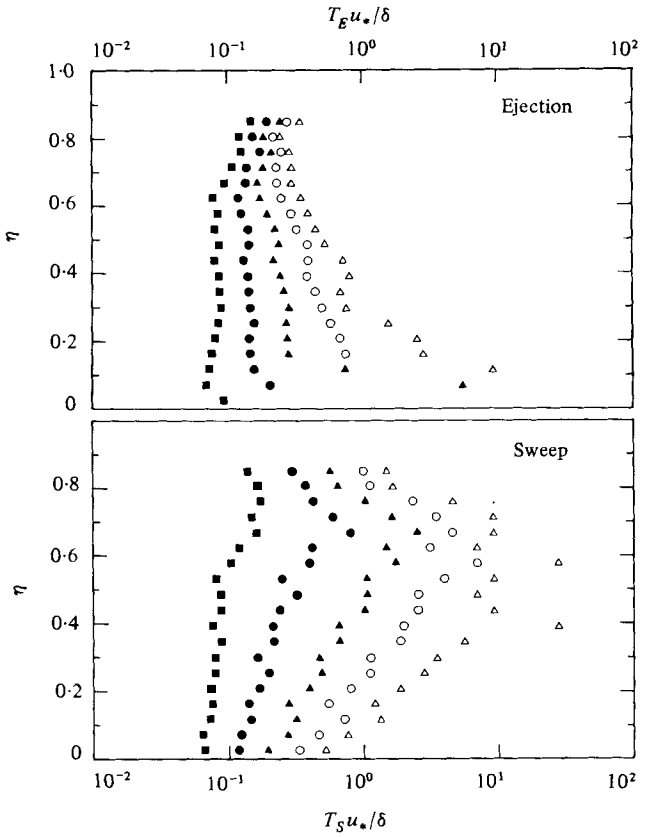

FIGURE 12. Ejection and sweep time scales T_E and T_S over surface F, for several different choices of trigger level H. ■, $H = 2$; ●, $H = 4$; ▲, $H = 6$; ○, $H = 8$; △, $H = 10$. Data from run 109.

6. Time and length scales of the turbulence

The procedure of Lu & Willmarth (1973) was used to investigate the effect of surface roughness on the time scales of the large turbulent structures. The method assumes that the short, intermittent periods of intense Reynolds stress which characterize turbulent boundary-layer flow are directly associated with the large structures discussed in § 1. Some evidence for this assertion comes from the work of Brown & Thomas (1977), which has already been mentioned. The implication is that the frequency with which large structures pass a given fixed point in the boundary layer is proportional to the frequency of suitably defined high-stress events at that point. The constant of proportionality depends on the event definition.

The number of ejection or sweep events in a record was counted by setting a threshold hole size H, and counting the number of negative crossings of the level $-H\overline{u'w'}$ by the series $u'(t)\,w'(t)$ with (u', w') in the appropriate quadrant; from this number, a mean time interval T_E or T_S between ejection or sweep events could be found. Clearly T_E and T_S depend upon the choice of H; figure 12 shows, for surface F, the variation of T_E and T_S with η for several different choices of H. Use of the method for absolute determination of time or length scales is therefore precluded. However, given a consistent choice for H, it is legitimate to compare values of T_E and T_S over different

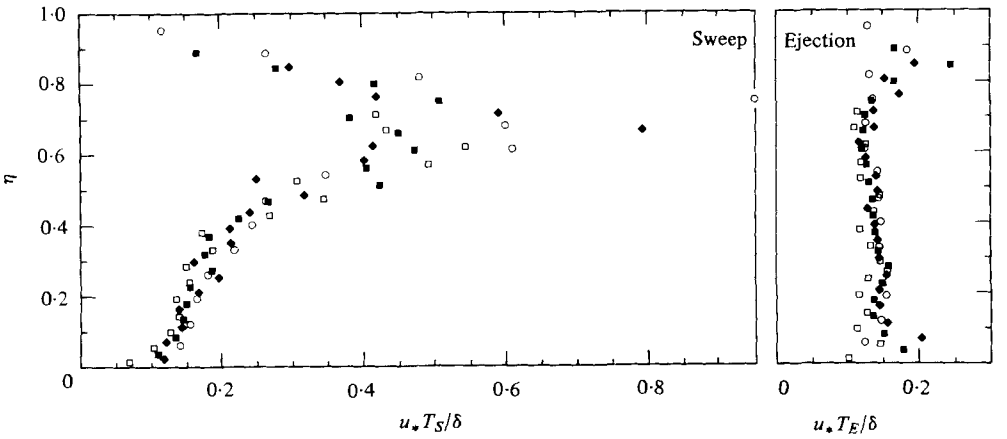

FIGURE 13. Ejection and sweep time scales T_E and T_S over surfaces A, C, E and F, with trigger level $H = 4$. Data from runs 10, 53, 79, 109. Symbols as in figure 4.

surfaces, because the moments and probability of distributions of u' and w' are universal, roughness-independent functions of η in the outer layer. Using the threshold $H = 4$ for both ejections and sweeps, figure 13 shows the variation with η of T_S and T_E for surfaces A, C, E and F. The abscissae are normalized as $u_*T_{S,E}/\delta$, which is clearly successful in collapsing data for all surfaces in the roughness-independent part of the flow ($\eta \gtrsim 0{\cdot}15$). Plots similar to figure 13, but using different values of the threshold H (e.g. $H = 2$, 6, 8, ...) verify that this normalization is equally successful for any choice of H.

It should also be noted that normalization of T_S and T_E as $U_\infty T_{S,E}/\delta$ is unsuccessful in collapsing the data. As u_*/U_∞ varies by a factor of nearly 2 from surface A to surface F, the resulting plot is a spread over a similar factor.

We now assume that, for given values of H and η, T_S and T_E are proportional to the time T separating the passage of consecutive large structures through a fixed point. The above results then show that a general property of zero-pressure-gradient turbulent boundary layers is that Tu_*/δ is a constant, independent of surface roughness. This somewhat modifies the often-quoted finding of Rao, Narisimha & Badri Narayanan (1971) that the time T scales with U_∞ and δ. In fact, there is no contradiction between the present results and those of Rao *et al.*, because their data were all obtained over a smooth surface by varying U_∞, with only small consequent change in u_*/U.

The only other information known to us about T_E over rough surfaces is the study by Sabot, Saleh & Comte-Bellot (1977) of fully developed smooth and rough wall pipe flow. They found that $T_E U_c/R_h$ (where U_c is the mean core velocity and R_h the hydrodynamic radius) increased with increasing surface roughness. At a trigger level of $H = 9$ (using the definition of this paper) and at $\eta = 0{\cdot}4$, their results give $u_*T_E/R_h = 0{\cdot}12$ for a smooth pipe and 0·68 for a rough pipe; in contrast, the present experiment gives $u_*T_E/\delta = 0{\cdot}50$ at $H = 9$, for all surfaces. The Reynolds numbers for the two experiments were almost identical. The apparent disagreement is probably a consequence of the different external conditions imposed on the two flows. Fully developed pipe flow occurs in a streamwise pressure gradient dependent on the roughness, and is governed by a length scale R_h which is geometrically fixed; zero pressure-gradient

turbulent boundary layers are governed by a thickness δ which increases with surface roughness, as shown in table 1.

It is of interest to compare the time scales found here with those from other work, although it must be borne in mind that no unambiguous signature for large structures in a single-point (or even multi-point) velocity record has yet been found; hence, estimates of the quantity TU_∞/δ vary by at least an order of magnitude. For example, Rao *et al.* (1971) concluded that $TU_\infty/\delta \approx 2{\cdot}4$ by counting periods of strong activity in a turbulence signal which had been passed through a narrow band-pass filter. Antonia, Danh & Prabhu (1976) summarize other estimates by the same and other techniques which give values between 0·5 (their own estimate) and 5. To obtain a value of T from the present work, we use the event 'ejection with $H = 4$', simply because figures 12 and 13 show that this event produces values of T_E which are independent of height outside the roughness sublayer. From figure 13, the appropriate constant value of T_E is given by $T_E u_*/\delta = 0{\cdot}13$, for all surfaces. (Figure 13 also shows that T_S is strongly height-dependent at $H = 4$, especially in the outer layer. This is not surprising, as it has already been shown that ejections are far more significant than sweeps as contributors to the total stress in the outer layer; it is therefore expected that intense sweeps are relatively rare events there.)

It is helpful to consider a length scale $L = U_\infty T$, the streamwise separation between consecutive large structures (where the advection velocity for large structures is assumed to be some fixed fraction of U_∞). Then, since $L/\delta = TU_\infty/\delta = 0{\cdot}13(U_\infty/u_*)$, we obtain $L/\delta = 3{\cdot}6$ (surface A), 2·4 (surface C) and 2·1 (surface F). That these values coincide so well with the experimental range of 0·5 to 5, and especially with Rao *et al.*'s value of 2·4, is merely fortuitous. The significant aspect, however, is that L/δ varies with surface roughness: as the strength of the momentum sink at the surface increases, *more* large structures develop per unit streamwise length of the boundary layer, where δ is the length scale.

7. Discussion

One implication of (11) and (12) is to relate the turbulent flux of turbulent kinetic energy

$$F_{TKE} = \tfrac{1}{2}(\overline{w'u'^2} + \overline{w'v'^2} + \overline{w'^3}) \tag{13}$$

to the ejection–sweep character of the Reynolds stress as parametrized by ΔS_0. If in the absence of measurements, $\overline{w'v'^2}$ is approximated by $\frac{1}{2}(\overline{w'u'^2} + \overline{w'^3})$ (cf. Antonia & Luxton 1971, p. 750) then

$$F_{TKE} = \tfrac{3}{4}\Delta S_0(c_1\sigma_u^2\sigma_w + c_2\sigma_w^3), \tag{14}$$

where $c_1 = (-2{\cdot}02 \times 0{\cdot}37)^{-1} = -1{\cdot}34$ and $c_2 = -1{\cdot}59$, from (11) and (12). It is clear that in the roughness sublayer where sweeps dominate and ΔS_0 is positive (see figure 9), F_{TKE} will be negative, implying a downward turbulent energy flux. Further, the decrease of ΔS_0 with increasing height in the roughness sublayer implies that the transport term $-\partial F_{TKE}/\partial z$ in the turbulent energy budget,

$$0 = -\overline{u'w'}\frac{\partial \bar{u}}{\partial z} - \frac{\partial}{\partial z}(\overline{p'w'} + F_{TKE}) - \epsilon \tag{15}$$

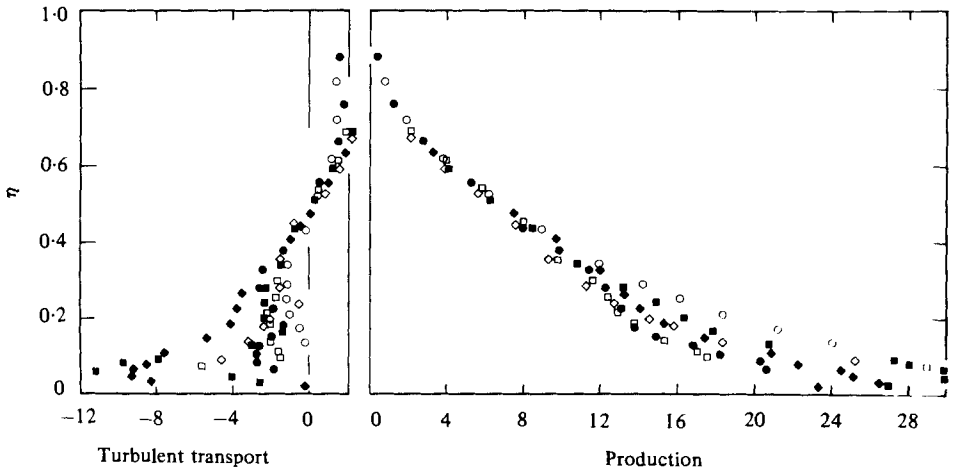

FIGURE 14. For each surface, average dimensionless production and transport terms in the turbulent energy budget, (15). Production term normalized as $-(\delta/u_*^3)\,\overline{u'w'}\,\partial\bar{u}/\partial z$; transport term as $-(\delta/u_*^3)\,\partial F_{TKE}/\partial z$, F_{TKE} being approximated by $\frac{1}{4}(\overline{w'u'^2}+\overline{w'^3})$. Symbols as in figure 1.

(where p' is the kinematic pressure fluctuation and ϵ the dissipation rate), represents a local turbulent energy loss. This is confirmed in figure 14, in which the production term and the transport term are plotted against η using the normalizing factor δ/u_*^3, appropriate to the outer layer. Close to surfaces E and F (at $z \approx h$) the plotted transport term represents a loss of about 30 % of the production term; this fraction decreases with falling roughness concentration to near zero for the smooth surface. These results are in agreement with existing turbulent energy balance information from smooth walls (e.g. Townsend 1976, p. 293) and from a three-dimensional, random, rough surface (Mulhearn & Finnigan 1978).

It is useful to compare the findings of the present experiment with data from the atmospheric surface layer. In the matched layer, in near-neutral conditions, it is known that skewnesses of u and w are small and that the uw distribution does not depart far from joint normality (Izumi 1971; Hennemuth 1978). Close to vegetated surfaces, on the other hand, the third moments of u and w are of considerable magnitude and are signed in accordance with figure 4. Maitani (1978) measured skewnesses for u and w of 1 and $-0{\cdot}5$, respectively, at the tops of wheat, rice and rush canopies, and observed typical turbulent energy fluxes F_{TKE} of $-2u_*^3$, directed downward. Finnigan (1979*a*) applied quadrant analysis to Reynolds-stress measurements above and within the canopy, obtaining ΔS_0 values between 0·3 and 1 at the top of the canopy and as high as 2 within the canopy, with significant contributions at very high values of H in the sweep quadrant (cf. figure 6). His data are in broad agreement with (12), despite considerable scatter imposed by a short averaging period of 5 min. It is clear that the behaviour found for the roughness sublayer in the present work is also observed in the atmosphere.

In interpreting observations within the roughness sublayer, allowance must be made for the spatial variability imparted by the three-dimensionality of the flow near the roughness. In the present experiment, lateral traverses were used to place limits on this variation, as described in I. For example, it was shown that, in the roughness sublayer *above* the canopy, the standard deviation of $\overline{u'w'}$ along a lateral traverse is

typically 5 % of the mean value of $\overline{u'w'}$ along the same traverse. This remarkably small variation was observed over all surfaces at heights such that $(z-h)/D \gtrsim 0{\cdot}1$, where D is the spacing between elements. The corresponding lateral variability of the third moments is somewhat higher, typically about 20 %. Nevertheless, this is small enough to give confidence that the features of the roughness sublayer described in this paper are of general applicability. Further evidence is provided by the agreement between these results and those from several different surface types, including atmospheric rough surfaces.

Finally, it must be noted that all surfaces considered here are 'k-type' roughness, in the notation of Perry, Schofield & Joubert (1969). It is possible that for 'D-type' roughness, in which nearly stable recirculating vortices are formed behind roughness elements (as for transverse bar roughness, for example), the dominance of sweeps in the roughness sublayer will not occur. Townsend (1976, p. 142) has speculated that ejections dominate the Reynolds stress close to this kind of roughness.

The experimental part of this work was carried out in the Department of Meteorology, University of Edinburgh, with financial support from the Natural Environment Research Council. Wind-tunnel facilities were generously loaned by the Director of the Fluid Mechanics Unit, Department of Physics, University of Edinburgh. I am indebted to the late Dr A. S. Thom for the opportunity to carry out this work, and for his perceptive encouragement during its experimental phase. I also thank the referees for their detailed comments.

REFERENCES

Antonia, R. A. & Atkinson, J. D. 1973 *J. Fluid Mech.* **58**, 581.

Antonia, R. A., Danh, H. Q. & Prabhu, A. 1976 *Phys. Fluids* **19**, 1680.

Antonia, R. A. & Luxton, R. E. 1971 *J. Fluid Mech.* **48**, 721.

Brown, G. L. & Thomas, A. S. W. 1977 *Phys. Fluids* **20**, S248.

Falco, R. E. 1977 *Phys. Fluids* **20**, S124.

Finnigan, J. J. 1979*a* *Boundary-Layer Met.* **16**, 181.

Finnigan, J. J. 1979*b* *Boundary-Layer Met.* **16**, 213.

Grass, A. J. 1971 *J. Fluid Mech.* **50**, 233.

Hennemuth, B. 1978 *Boundary-Layer Met.* **15**, 489.

Izumi, Y. 1971 *Kansas* 1968 *Field Program Data Report.* Environmental Research Paper no. 379, Air Force Cambridge Research Laboratories, Cambridge, Massachusetts.

Kim, H. T., Kline, S. J. & Reynolds, W. C. 1971 *J. Fluid Mech.* **50**, 133.

Kovasznay, L. S. G. 1977 The role of large-scale coherent structures in turbulent shear flows. In *Proc. 5th Biennial Symp. on Turbulence.* Princeton: Science Press.

Kovasznay, L. S. G., Kibens, V. & Blackwelder, R. F. 1970 *J. Fluid Mech.* **41**, 283.

Lu, S. S. & Willmarth, W. W. 1973 *J. Fluid Mech.* **60**, 481.

Maitani, T. 1978 *Boundary-Layer Met.* **14**, 571.

Mulhearn, P. J. & Finnigan, J. J. 1978 *Boundary-Layer Met.* **15**, 109.

Nakagawa, H. & Nezu, I. 1977 *J. Fluid Mech.* **80**, 99.

Nychas, S. G., Hershey, H. C. & Brodkey, R. S. 1973 *J. Fluid Mech.* **61**, 513.

Perry, A. E., Schofield, W. H. & Joubert, P. N. 1969 *J. Fluid Mech.* **37**, 383.

Rao, K. N., Narasimha, R. & Badri Narayanan, M. A. 1971 *J. Fluid Mech.* **48**, 339.

Raupach, M. R. & Thom, A. S. 1981 *Ann. Rev. Fluid Mech.* **13**, 97.

Raupach, M. R., Thom, A. S. & Edwards, I. 1980 *Boundary-Layer Met.* **18**, 373.

SABOT, J., SALEH, I. & COMTE-BELLOT, G. 1977 *Phys. Fluids Suppl.* **20**, 150.

TENNEKES, H. & LUMLEY, J. L. 1972 *A First Course in Turbulence.* Massachusetts Institute of Technology Press.

TOWNSEND, A. A. 1976 *The Structure of Turbulent Shear Flow*, 2nd edn. Cambridge University Press.

WALLACE, J. M., ECKELMANN, H. & BRODKEY, R. S. 1972 *J. Fluid Mech.* **54**, 39.

WILLMARTH, W. W. 1975 *Adv. Appl. Mech.* **15**, 159.

WILLMARTH, W. W. & LU, S. S. 1974 *Adv. Geophysics* A **18**, 287.